



Heterogeneous Fenton-Like Catalytic Degradation of Remazol Brilliant Violet Dye Using Starch-Fe⁰Nps-Silica Composite

Vandana Singh*, Jadveer Singh and Preeti

*Department of Chemistry, University of Allahabad, Allahabad-211002, **INDIA**

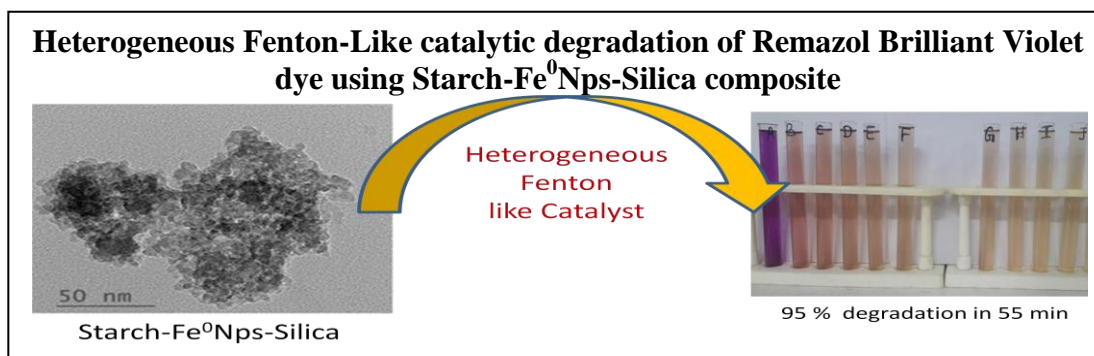
Email: singhvandanasingh@rediffmail.com

Accepted on 13th October 2017, Published online on 27th November 2017

ABSTRACT

Fenton-like degradation of Remazol Brilliant Violet dye (RBV) has been carried out using Starch-Fe⁰-Silica catalyst. A series of starch-zerovalent iron-silica composites (SFS₁ to SFS₈) with different starch/Fe⁰/silica ratios were prepared using an inexpensive and simplistic sol gel technique and mango leaf reduction strategy. In preliminary experiments SFS₁ showed optimum performance towards the dye degradation, therefore this sample was used for detailed characterization using HR-TEM, EDX, FE-SEM and FTIR techniques. The presence of starch and silica minimized the agglomeration of Fe⁰ nanoparticles. The results of HR-TEM study showed that SFS₁ has spherical Fe⁰ nanoparticles of approx. 4 nm average size. The dye degradation was initially fast and 79 % dye was degraded from 100 mg L⁻¹ dye solution using 0.05 g of catalyst dose, in first five min. As the time passed the degradation eventually slowed down and almost 90% dye was degraded within 55 min. The degradation kinetic data obeyed pseudo first order kinetic model with rate constant 0.03224 min⁻¹. The catalyst performed efficiently well over a wide range of dye concentrations (25-200 mg L⁻¹). The catalytic efficiency of St-Fe⁰-Si remained significant up to four repetitive cycles, that evidenced its strong catalytic potential.

Graphical Abstract



Keywords: Fenton-like catalytic degradation, Remazol Brilliant Violet dye (RBV), Starch-Fe⁰Nps-Silica Composite.

INTRODUCTION

Today's world is endangered from toxic effluents of industries [1], especially the dye industries. These effluents are one of the major causes of water contamination [2] as dyes are colored, toxic, non-biodegradable and xenobiotic. The conventional techniques of dye removal, such as physical, biological and light degradation [3,4,5] are not efficient as they only concentrate the dye molecules to another phase, exhibit lower efficiency, consume more energy, and require secondary methods to complete the elimination process. The presence of dye molecules in water bodies can deplete the dissolved oxygen and retard the growth of aquatic biota by interrupting the sunlight. Hazardous reactive dyes have shown toxicity to many organs such as brain, skin, eyes, throat, liver, kidney, respiratory, and reproductive system. Therefore, it is necessary to develop proficient novel techniques for dye remediation which also have high efficiency and low cost.

The metal nanoparticles have attracted widespread attention as catalysts because of their unique electronic and surface properties, and also due to their high surface-to-volume ratios [6,7]. Zerovalent iron nanoparticles (Fe^0) are accepted as efficient catalyst for degradation of non-biodegradable harmful reactive dye molecules. Its favorable characteristics include: high specific surface area, cost effectiveness, high reactivity as a strong reductant and ability to trigger the generation of reactive oxygen species through the Fenton reaction [8-10]. Fenton processes have been used as the potent source of hydroxyl radicals from H_2O_2 in the presence of $\text{Fe}^{2+}/\text{Fe}^{3+}$ and have been utilized for degrading the organic pollutants with high efficiency [11]. Nevertheless, there are quite a few demerits associated with the application of homogeneous Fenton processes which include tedious recycling of catalyst and high cost. Further, the treatment of iron-containing sludge, present in discharges, adds to the demerits of this application. These drawbacks have triggered the development of heterogeneous Fenton catalysts using iron nanoparticles but the high surface energies and intrinsic magnetic interactions of iron nanoparticles pose fatal shortage to this development in the form of oxidation (by nearby media e.g., dissolved oxygen) or agglomeration. This results in the fast inactivation of mobility, chemical reactivity and surface area of the nanoparticles [14]. To avoid the aforementioned problems, various supports such as biochar [15], clay [16], graphene [17], zeolites [18,19], silica [20,21], mesoporous carbon composites [22], mesoporous silica [23], activated carbon [24], montmorillonite [25], polysaccharide [26-28] etc. have been used to stabilize the Fe^0 nanoparticles.

In the present study, a simplistic two step procedure has been evolved to fabricate heterogeneous Fenton like catalyst, starch- Fe^0 Nps-silica composite (SFS). The use of starch and silica was prompted because of their low cost and environmental friendliness. The Fe^0 Nps were first synthesized as a result of reduction with mango leaf extract (*Mangifera indica*) and was subsequently hybridized with starch and silica using sol gel method to obtain the catalyst. Starch is a nontoxic, biodegradable and economical biopolymer which is abundant in nature. It contains a group of polysaccharides, composed of glucopyranose units that are mutually connected through glycosidic linkages. The prepared starch- Fe^0 -silica composite catalyst was used as the heterogeneous Fenton catalyst for the degradation of the Remazol Brilliant Violet dye (azo dye).

MATERIALS AND METHODS

Chemicals and instrumentation: Analytical reagents of tetraethylorthosilicate (98% TEOS; Merck, Germany), Soluble starch, Ferric nitrate (Merck), hydrogen peroxide (H_2O_2 , 30 wt %), NH_4OH (30% NH_3 ; Merck) were purchased from Merck, India. Absolute ethanol 99.9% (AR) was from Changshu Yangyuan Chemical, China. Double distilled water was used in all the procedures. The pH values were adjusted with the help of 5 M HCl (Merck); or 1 M NaOH (Merck). EUTECH Instruments pH meter (model 510) was used for the pH measurements. Orbital shaker Incubator, Metrex Scientific Instruments (P) Ltd., New Delhi was used. Field Emission Scanning Electron Microscopy (FE-SEM) of the composites was performed using FESEM/EDX (SUPRA 40 VP) instrument. The samples were coated with gold to avoid

charging. High Resolution Transmission Electron Microscopy, EDX and elemental mapping was conducted using a FEI Titan G2 60-300 TEM (HR-TEM) instrument. The sample was dispersed in ethanol and the dispersed sample was sonicated before placing on the grids for the HR-TEM analysis. UV-visible spectrum was recorded on a Cyber Lab double beam UV-visible spectrophotometer. FTIR was done on Perkin Elmer FTIR spectrophotometer.

Synthesis of Fe⁰Nps: Fe⁰Nps have been crafted using a mango leaf extract (*Mangifera indica*) reduction method [29]. In brief, 1 g of dried mango leaves were boiled in 25 ml distilled water until volume was reduced to 10 ml. The extract was filtered and collected in a clean beaker (leaf extract). The leaf extract was then added dropwise to 0.1M Ferric nitrate solution in 1:1 volume ratio. Immediately after addition of the leaf extract, the color of the ferric nitrate solution turned black which indicated the formation of zerovalent iron nanoparticles (Fe⁰Nps). Their formation was further evidenced by the appearance of strong SPR absorption peaks (at 225 nm and 265 nm) in UV-VIS spectrum of the solution.

Synthesis of catalyst (Starch-Fe⁰Np-silica composite): A known weight starch (0.05 - 0.2 g) was dissolved in a known volume (6.5 -10 ml) of distilled water in 50 ml conical flask under magnetic stirring to obtain a homogenous solution of starch. Separately, a known volume of TEOS was mixed with a known volume of EtOH and this mixture was subsequently added to the starch solution of known concentration (w/v). The mixture was stirred on a magnetic stirrer at room temperature for 10 minutes. The known volumes of Fe⁰Nps and 12 N ammonium hydroxide solutions were rapidly added to this stirred mixture and the stirring was continued till a hybrid gel was obtained. The whole process was carried out at room temperature. The gel was dried and powdered in an electric oven at 40 °C and used as catalyst.

Synthesis of the controls: The starch-silica composite (St-Si) and control silica (CS) were synthesized by the same procedure as mentioned above. St-Si have been synthesized by using 0.05 g starch, 10 mL of H₂O, 2.5 mL TEOS, 2.5 mL EtOH and 1.5 mL of 12 N NH₄OH followed by stirring at room temperature till the hydrogel was formed. Similarly control silica (CS) were fabricated by sol gel method using 2.5 mL TEOS, 2.5 mL EtOH, 10 mL of H₂O and 1.5 mL of 12 N NH₄OH solution as catalyst. The resulting mixture was stirred till the hydrogel was obtained which was dried.

Catalytic performance: Stock solution of 1000 mg L⁻¹ was prepared by dissolving 1 g Remazol Brilliant violet dye in 1000 mL distilled water, which was later diluted with requisite volume of distilled water to achieve a desired initial concentrations (25 to 200 mg L⁻¹). A series of batch experiments were conducted on a temperature controlled incubator shaker set at 150 rpm and maintained at 35±2 °C for 55 min to measure the catalytic activity of the samples. The catalytic degradation of RBV dye was studied as a function of pH (2-8), catalyst dose (0.02-0.08 g), initial dye concentration (25 to 200 mg L⁻¹) and temperature (20-50 °C). The catalyst was added to the dye solution (100 mg L⁻¹) and the reaction medium was maintained to a known pH using an appropriate volume of 1 M NaOH or 5 M HCl. Subsequently, 1mL of H₂O₂ (3 M) was added to the above suspension and the degradation reaction was initiated. The flasks were kept in a temperature controlled orbital shaker with constant stirring during the reaction. Each flask was shaken for a desired time and the suspensions were filtered using Whatman 0.45 mm filter paper and the supernatants were analyzed for the remaining dye concentrations spectrophotometrically at 560 nm wavelength using UV-visible spectrophotometer. The catalytic degradation of RBV dye was calculated by the difference between the initial and the final readings using the following equation:

$$\% \text{ degradation} = (C_0 - C_e)/C_0 \times 100$$

C₀ is the initial dye concentration (mg L⁻¹), C_e is the equilibrium concentration of the dye in solution (mg L⁻¹). Averages and standard deviations were obtained from duplicate experiments which were less than 3 %.

RESULTS AND DISCUSSION

Synthesis of the starch-Fe⁰Np-silica composite (SFS): Fe³⁺ ions were reduced into Fe⁰ nanoparticles using mango leaf extract. The formation of the zerovalent iron nanoparticle was visualized by change in color of the ferric nitrate solution from yellow to black. Mango leaf extract was used as a reducing agent. Mango leaf extract was added to freshly prepared Fe(NO₃)₃·9H₂O solution in 1:1 ratio. The formation of iron nanoparticles was evidenced by the appearance of SPR peaks of ZVI Nps at 225 nm and 265 (Fig. 1 (a)) [30] and by visible change in the color of the solution from yellow to black.

The catalyst was crafted by adding known volumes of tetraethoxysilane (TEOS) and ethanol (EtOH) to the starch solution of known concentration. To this mixture, known volumes of 12 N NH₄OH and Fe⁰ Nps solution were added (Table. 1). The mixture was stirred for a known time period till the hybrid hydrogel was formed. The dried and powdered samples were evaluated for their catalytic activity for the dye degradation. The optimum sample (SFS) in terms of homogeneity and gelling time and dye degradation was obtained when the ratio of Fe⁰Nps: TEOS: EtOH: H₂O: NH₄OH was 2: 1.66: 4.66: 1 (Table. 1). The presence of Fe⁰Nps had an expediting influence on the sol-gel polymerization of TEOS and this significantly minimized the gelling time.

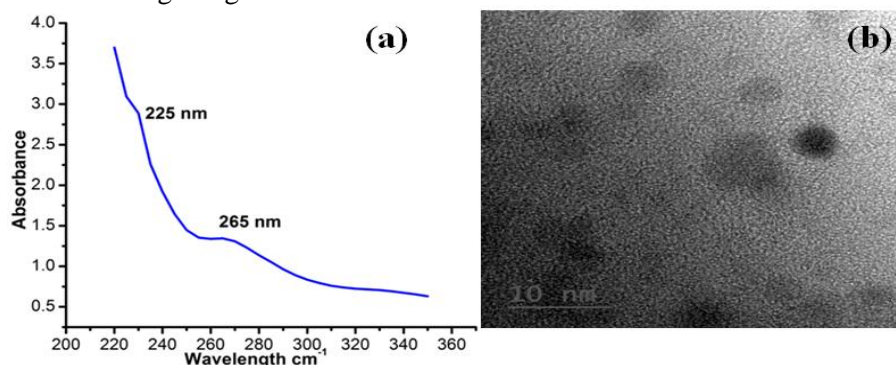


Fig. 1(a) UV-Visible spectrum (b) HR TEM image of Fe⁰ nanoparticle

Table 1. Optimization of catalyst synthesis by varying various process parameters while keeping the total reaction volume fixed (16.5 mL); dye degradation was done in batch adsorption experiment using 0.05 g catalyst, 20 mL of 100 mg L⁻¹ dye solution, 1 mL of H₂O₂ (3M), temperature 35°C, contact time 55 minute, rpm150, and pH 2.

Hybrid	Starch (g)	H ₂ O (mL)	TEOS (mL)	EtOH (mL)	Fe ⁰ Nps (M)	NH ₄ OH (mL)	Gel/ppt time (min)	Dye degradation (%)
CS	-	10	2.5	2.5	-	1.5	1080	0
St-Si	0.05	10	2.5	2.5	-	1.5	1055	0
SFS₁	0.05	7	2.5	2.5	0.1	1.5	26	89.50
SFS ₂	0.10	7	2.5	2.5	0.1	1.5	26	86.55
SFS ₃	0.15	7	2.5	2.5	0.1	1.5	26	84.75
SFS ₄	0.20	7	2.5	2.5	0.1	1.5	26	83.55
SFS ₅	0.05	9	1.5	1.5	0.1	1.5	31	81.41
SFS ₆	0.05	8	2.0	2.0	0.1	1.5	29	85.55
SFS ₇	0.05	6	3.0	3.0	0.1	1.5	ppt	87.90
SFS ₈	0.05	7	2.5	2.5	0.2	1.5	ppt	85.00
SFS ₉	0.05	7	2.5	2.5	0.3	1.5	ppt	83.51
SFS ₁₀	0.05	7	2.5	2.5	0.4	1.5	ppt	82.43
SFS ₁₁	0.05	8	2.5	2.5	0.1	0.5	40	86.42
SFS ₁₂	0.05	7.5	2.5	2.5	0.1	1.0	27	87.25
SFS ₁₃	0.05	6.5	2.5	2.5	0.1	2	26	88.17
FS	0.05	7	2.5	2.5	0.1	1.5	26	79.98

Characterization of St-Fe⁰Np-Si hybrid

UV/Visible spectrum: The degradation of Remazol Brilliant violet dye was monitored with the help of UV-Vis absorption spectroscopy. RBV dye has intense violet color due to the presence of naphthalene rings (aromatic rings) in conjugation with azo group (-N=N-) and $\pi-\pi^*$ transitions give rise to two characteristic absorption peaks at 325 nm and 560 nm [31, 32] (Fig. 2). The intensity of the absorption peak at 560 nm decreased rapidly within 5 min time after the addition of catalyst (SFS₁) and the peak nearly disappeared in 55 min. This indicated the possible cleavage of the azo bond and destruction of the conjugated π system. The peak observed at 230 nm corresponded to the formation of aromatic products [33] while the weakening of absorption peak at 230 nm reflected the degradation of naphthalene and benzene derivatives. As no new absorbing peak appeared in the region 300 to 700 nm, it can be predicted that the reaction intermediates (produced during the reaction progression) neither have any conjugated system nor they possess any new chromophoric group. The azo bond was broken within 5 min and ~90 % dye degradation was possible in 55 min. It is indicated that the azo bonds (-N=N-) are much more prone to degradation (by hydroxyl radicals) than the aromatic rings. This is evidenced by faster decolorization than the complete mineralization of the azo dye [34, 35].

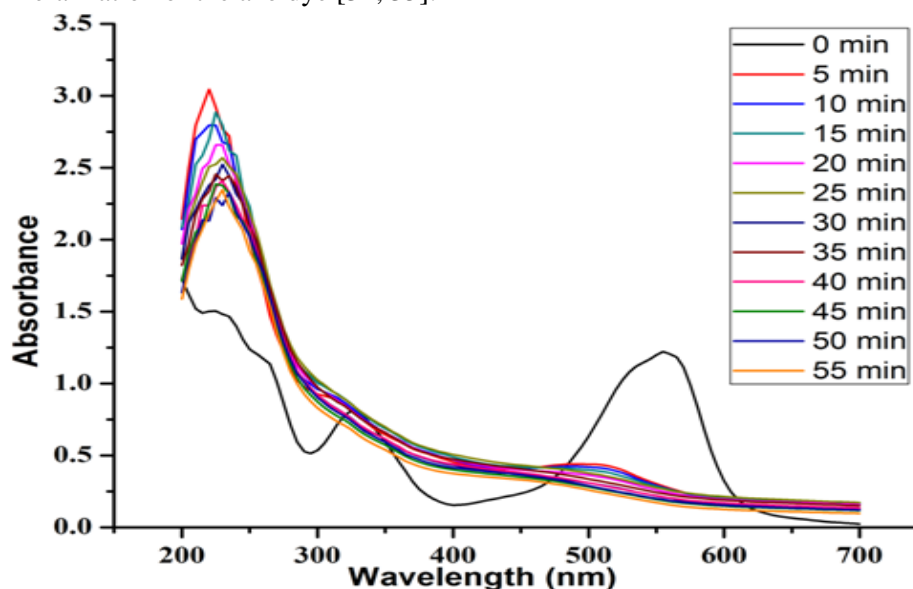


Fig. 2: UV/Vis absorption measurement of Remazol brilliant Violet dye degradation

Fourier Transform Infrared Spectroscopy: The FTIR spectrum of pure starch (Fig. 3 (a)) showed absorption at 3419 cm^{-1} (stretching of -OH groups), 2918 cm^{-1} (C-H stretching), 1649 cm^{-1} (COO^- asymmetric stretching), and 1417 cm^{-1} (COO^- symmetric stretching). The stretching peaks due to C-O bond are seen at 1158 cm^{-1} , 1081 cm^{-1} and 1016 cm^{-1} while the peaks at 928 cm^{-1} , 859 cm^{-1} , 764 cm^{-1} and 574 cm^{-1} corresponded to the anhydroglucose ring stretching vibrations [36].

Silica incorporation in the starch was confirmed by the appearance of SiO-H, Si-OH, and O-Si-O absorption peaks at 3437 cm^{-1} , 971 cm^{-1} , 1071 cm^{-1} and 799 cm^{-1} respectively (Fig. 3 (b)) [37]. Silanol O-H stretching peak is seen merged with starch O-H stretching peak at 3437 cm^{-1} . The peak observed at 466 cm^{-1} (bending vibrations) signified the formation of siloxane domains (SiO_4) [38].

In FTIR spectrum of catalyst (SFS₁), the SiO-H, Si-OH and O-Si-O stretching are seen at 3451 cm^{-1} , 970 cm^{-1} , 1087 cm^{-1} , 469 cm^{-1} and 797 cm^{-1} respectively. Peak observed at 1637 cm^{-1} is a characteristic of COO^- asymmetric stretching of polysaccharide (Fig. 3 (c)).

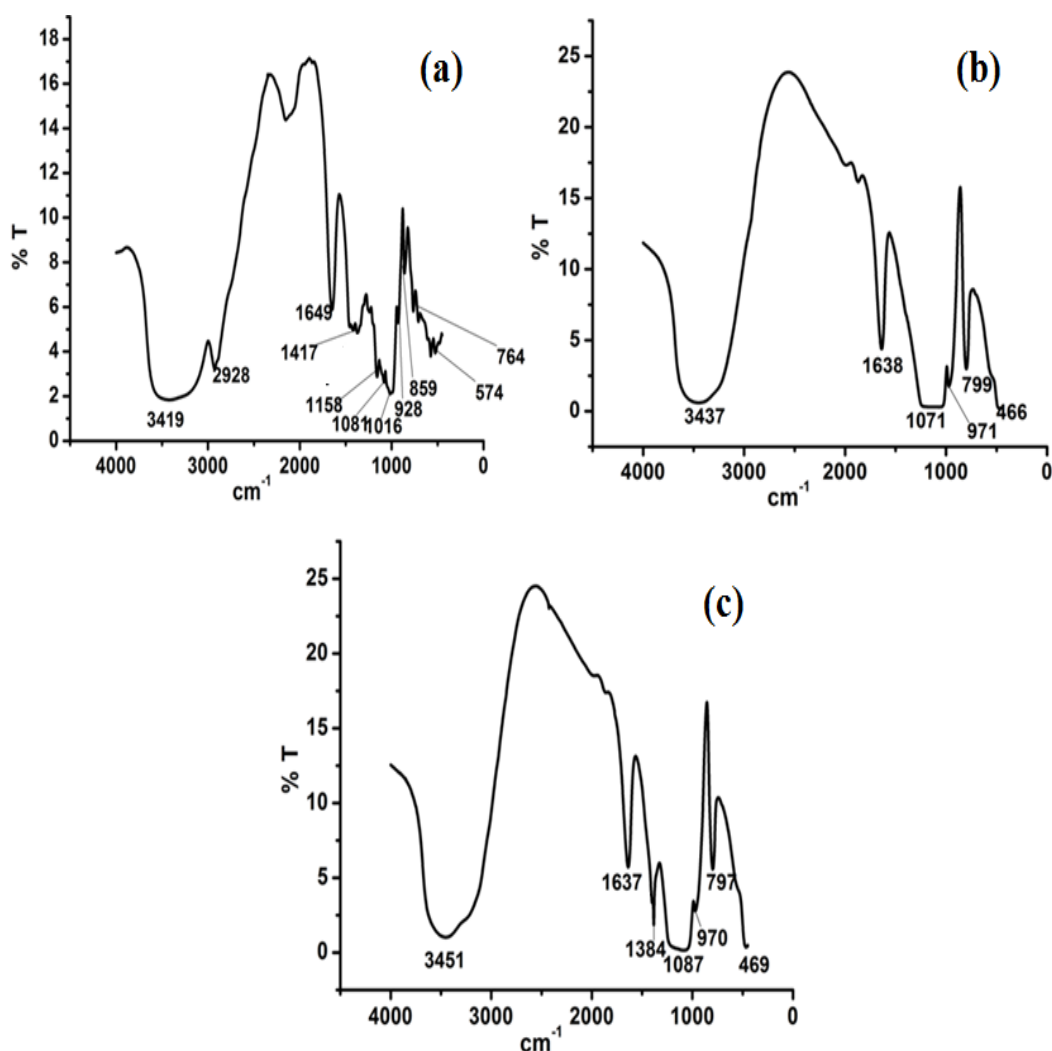


Fig. 3 FTIR spectra (a) Starch (St) (b) St- Si (c) St- Fe⁰-Si catalyst (SFS₁)

High Resolution Transmission electron microscopy (HR-TEM) and Energy Dispersive X-ray Analysis (EDX): Fig. 4 (a) and (b) shows the HR-TEM images of St-Si composite and SFS₁ (catalyst). St-Si composite observed as a cluster of large globular particles (silica nanoparticles) (Fig. 4(a)). The HR-TEM micrograph of the synthesized catalyst (SFS₁) showed that the Fe⁰Nps are dispersed within starch-silica matrix and have a relatively dense and non-uniform distribution (Fig. 4(b)). HR-TEM images revealed that the crystalline Fe⁰ nanoparticles are nearly spherical in shape. HR-TEM images of catalyst at different magnification are shown in Fig. 5. HR-TEM histogram (Fig. 5 (b) showed that the Fe⁰ nanoparticles have an average particle size of about 4 nm. The high resolution TEM (HRTEM) image of optimum sample shows lattice fringes having d-spacing of 0.202 nm which is in good agreement with the body-centered cubic iron (110) plane of Fe⁰ nanoparticles (Fig. 6) [39]. Fig. 7 and Fig. 8 present the EDX mapping and element analysis of St-Si and SFS₁. EDX spectrum the composite (starch-silica) revealed that it consists of carbon, oxygen, and silicon (Fig. 7 (e)). EDX spectrum of SFS₁ indicated it has iron, carbon, oxygen, and silicon. Fig. 8 (f) shows that the percentages of C, O and Si are higher than Fe which is shown as tiny peak of Fe. The presence of carbon, silicon and oxygen represented the presence of starch and silica. The element distribution of Fe, Si, O and C in SFS₁ has been done by element mapping analysis (Fig. 7 (a-d) and Fig. 8 (a-e)). The mapping shape of iron, silica, carbon, and oxygen elements showed that they are evenly distributed throughout the composite (SFS₁ and St-Si).

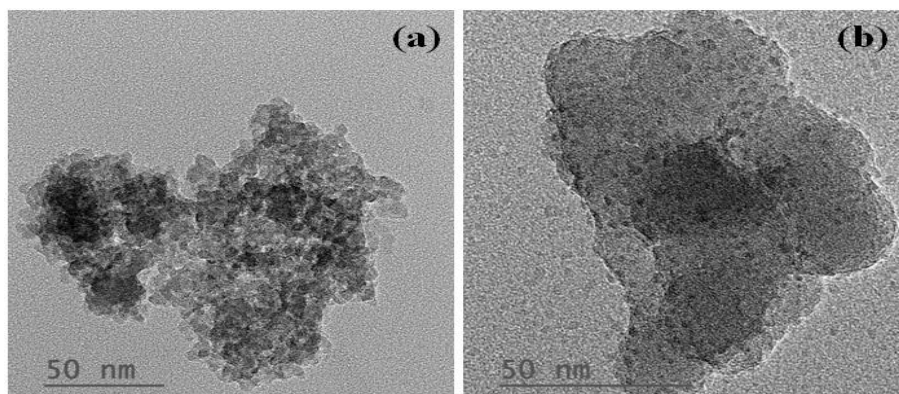


Fig. 4: HR- TEM micrograph of (a) St-Si hybrid and (b) St-Fe⁰-Si catalyst (SFS)

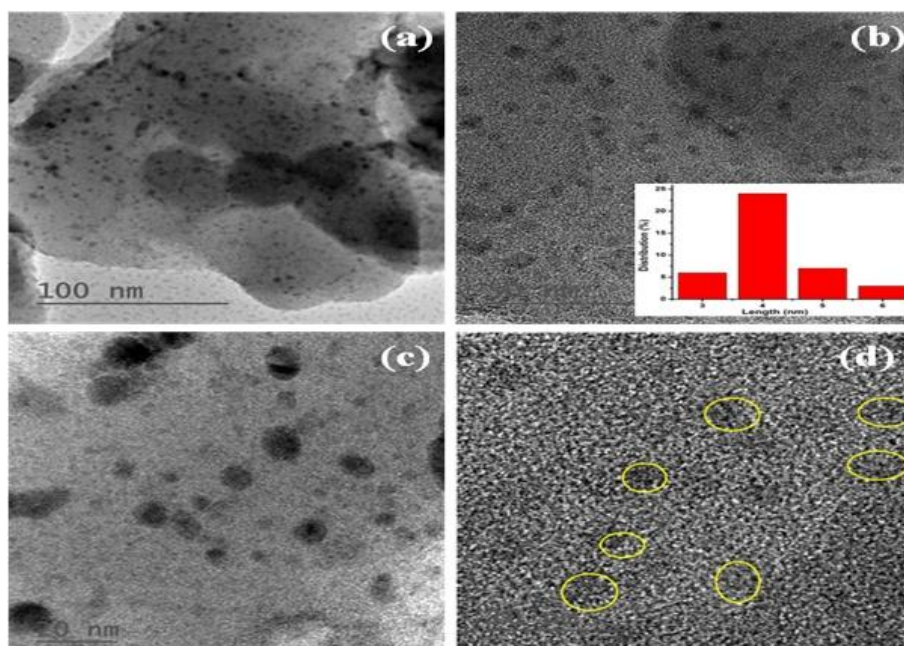


Fig. 5: High Resolution Transmission electron micrographs of catalyst at different magnification and Histogram seen as inset of (b)

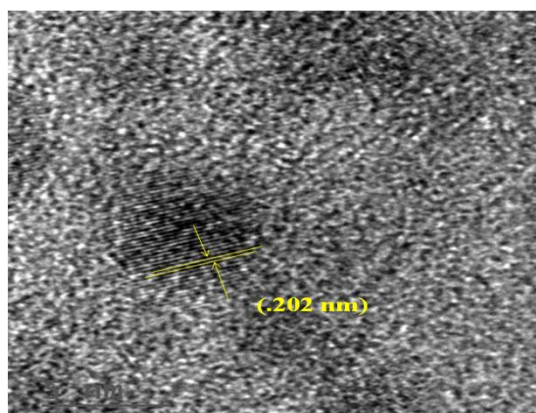


Fig. 6: HR-TEM image showing fringes with an interplanar distance of 0.202 nm

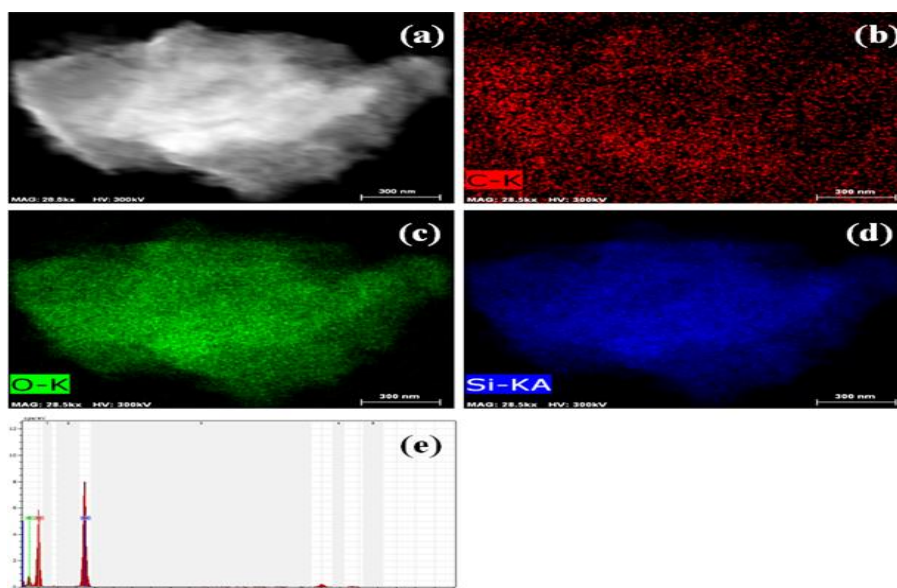


Fig. 7: (a) HAADF HR-TEM image of St-Si and its corresponding elemental mappings for (b) C, (c) O and (d) Si, (e) The corresponding EDX spectrum taken from the whole area of (a)

Field Emission Scanning Electron Microscopy: FE-SEM images of starch, St-Si, SFS₁ are depicted in Fig. 9. FE-SEM micrographs of starch revealed a smooth surface morphology with oval or ellipsoidal, and spherical shaped microparticles as observed by Odeku and Picker [40] (Fig. 9 (a)). St-Si showed rough surface that suggested that the small silica particles are deposited at the surface of starch (Fig. 9(b)). It can be seen that (Fig. 9(c)) the surface of composite (SFS₁) is dispersed with Fe⁰ nanoparticles (somewhat agglomerated) which are spherical in shape. The zerovalent nanoparticles are not separately seen, may be due to their very small amount. Fig. 10 shows the FESEM micrographs of catalyst at different magnification.

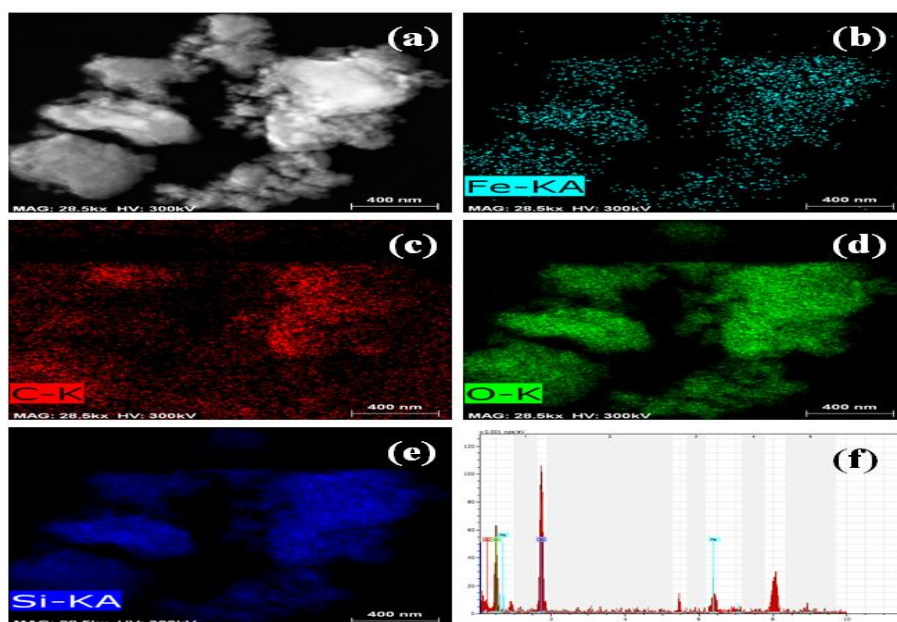


Fig. 8: (a) HAADF HR-TEM image of SFS₁ and its corresponding elemental mappings for (b) Fe, (c) C, (d) O and (e) Si, (f) The corresponding EDX spectrum taken from the whole area of (a).

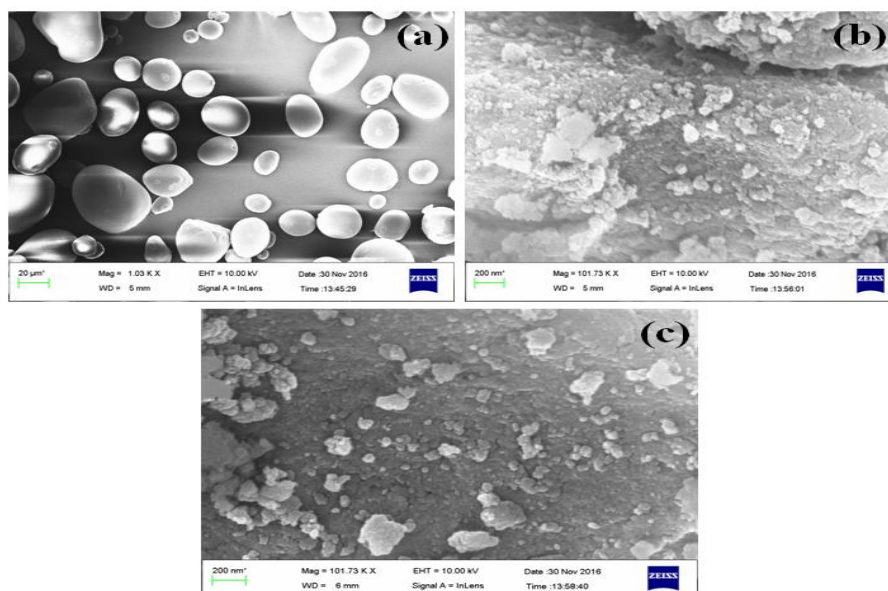
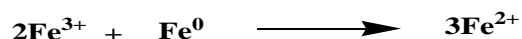
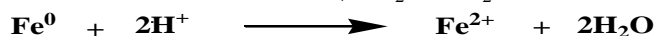


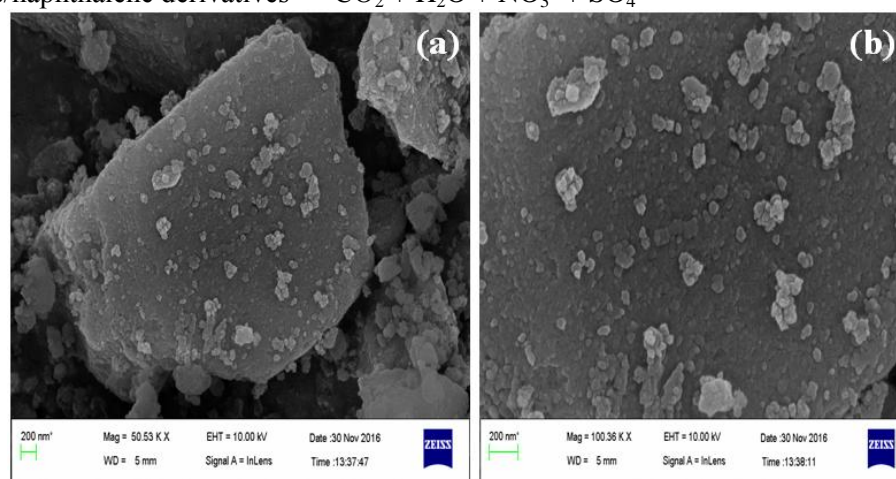
Fig. 9: (a) FE-SEM image of (a) Starch (St), (b) St-Si, (C) St-Fe₀Np-Si (SFS)

Suggested mechanism for the dye degradation: The dye degradation by catalytic oxidation using SFS₁ as catalyst can be explained in following steps – Fe⁰ was/were converted into Fe⁺² ions under aqueous acidic condition and were subsequently released within the dye solution. SFS₁ acted as a heterogeneous catalyst (Fe reservoir) in the dye degradation process. The oxidized Fe²⁺ was further oxidized to Fe³⁺ in the presence of H₂O₂ and produced hydroxyl radicals and hydroxyl anion. Hydroxyl radicals attacked the azo bond (-N=N-) of RBV dye molecules to generate intermediates such as benzene and naphthalene derivatives. OH[•] attacked the C-NH₂ and C-SO₃H bond of different intermediates to finally convert the dye molecule to their most stable oxidation state i.e., CO₂ and H₂O and oxidized inorganic anions.



OH[•] + Remazol brilliant violet dye → benzene derivative/naphthalene derivatives

OH[•] + benzene/naphthalene derivatives → CO₂ + H₂O + NO₃⁻ + SO₄²⁻



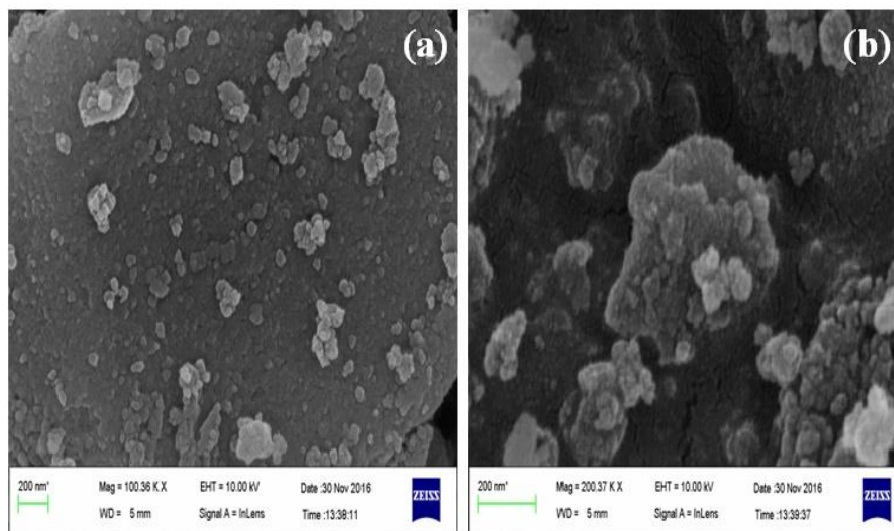


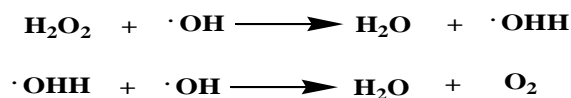
Fig. 10: Field Emission Scanning Electronmicrographs of catalyst at different magnification

Control studies for Dye removal: The batch experiments were performed using H_2O_2 and SFS_1 , independently, and SFS_1 in combination with H_2O_2 to evaluate the catalytic performance of the SFS_1 . When H_2O_2 was used in absence of catalyst, no dye degradation was witnessed after a passage of 55 min. This observation can be explained in two ways: i) the oxidizing power of hydrogen peroxide ($E_0 = 1.78 \text{ V}$) may be not enough for direct oxidation of RBV [41]; ii) in the absence of catalyst, the hydroxyl radical, which has greater oxidation potential ($E_0 = 2.85 \text{ V}$) is not formed in sufficient quantity. The results are in good agreement with the observation of other researchers [42]. In absence of H_2O_2 , SFS_1 could degraded 65 % dye in 55 min. This indicated that SFS_1 is capable of doing the reducing degradation of dyes. The addition of H_2O_2 improved the catalytic degradation as now 89.5 % dye degraded in 55 min. It is noteworthy that Fenton's process, which takes place in presence of hydrogen peroxide, is more effective for RBV dye degradation as compared to reducing degradation of dye. Such batch experiments clearly evidenced the role of every reagent in the degradation process.

Optimization of the dye degradation: The effect of various process parameters of dye degradation, like pH, initial dye concentration, catalyst (SFS_1) dose, $[\text{H}_2\text{O}_2]$, and temperature was investigated.

Effect of catalyst dosage: The effect of the initial catalyst dose on RBV dye decolorization was determined in the catalyst dose range of 0.02 g to 0.08 g. The results of percentage dye degradation are shown in Fig. 11 (a). The degradation increased (from 76.25 % to 89.5 %) on increasing the catalyst dose from 0.02 g to 0.05 g. The ease of access of Fe^0 was greater at higher dose of catalyst. This enhanced the production of Fe^{+2} and active sites on SFS_1 which produce extra free hydroxyl radical for the enhancement of decolorization rate of RBV dye.

Effect of H_2O_2 concentration: Degradation of dye at different hydrogen peroxide concentrations (1M to 10 M) was analyzed and the results are depicted in Fig. 11 (b). The degradation increased from 79.9% to 89.5% with the increase in the H_2O_2 concentration from 1M to 3 M at pH 2, 150 rpm, 0.05 g SFS_1 dose, contact volume 20 mL, contact time 50 min, temperature 35°C . This is explainable as at higher H_2O_2 concentrations, more hydroxyl radicals were generated. However, when concentration of hydrogen peroxide was $>4 \text{ M}$, the degradation of dye dropped down (from 88.08 % to 85.66 %) due to the formation of perhydroxy radicals, which further reacted with OH^\cdot to produce H_2O and O_2 . So it was concluded that high concentration of H_2O_2 behaved as scavenger of hydroxyl radicals and hence the oxidation was decreased [43]. The reaction can be presented by the following equation:



Effect of pH: It is known that pH is a deciding factor in Fenton degradation process. The effect of pH was studied in the range of pH 2 to pH 8 (Fig. 11 (c)). The pH of the dye solution affected the activity of the catalyst, speciation of iron, and decomposition of hydrogen peroxide [44]. The results accorded well with the classic Fenton process, in which acidic medium [45] is favorable for the oxidization of hydroxyl radical and hydrogen peroxide. However, degradation rate became poorer when pH was raised above pH 3. It was found that with the increase in pH from 3 to 8, the degradation rate decreased from 52 % to 36.5 %. At high pH values, H_2O_2 decomposed in to molecular oxygen and H_2O , rather than forming hydroxyl radicals, and accordingly the oxidizing ability of H_2O_2 was lost [46].

Effect of reaction temperature: To determine the effect of temperature on the dye degradation, a series of batch experiments were conducted between 20 °C to 50 °C. The results are depicted in Fig. 11 (d)., The dye degradation increased from 77.25 % to 89.5 % with the increase in temperature from 20 °C to 35 °C. When the temperature was further increased (> 35 °C), the degradation decreased. The degradation % ranged from 89.5 % to 84.83 % when the temperature was raised from 35 °C to 50 °C. This decrease can be attributed to thermal decomposition of H_2O_2 into oxygen and water [47].

Effect of the initial concentration of Remazol Brilliant Violet: In order to examine the effect of initial dye concentration on the degradation process, 0.05 g of catalyst was added into 20 mL solutions of RBV dye (initial concentrations ranging from 25 to 200 mg L^{-1}) at pH 2, 150 rpm, reaction time 55 min, and temperature 35°C. The effect of initial dye concentration on percentage dye degradation is shown in Fig. 11 (e). The degradation decreased from 98.91 to 85.11% on increasing the concentration from 25 to 200 mg L^{-1} .

Degradation kinetics: The kinetic study was performed in order to understand the dye degradation mechanism. The degradation of Remazol Brilliant Violet was analyzed using SFS₁ composite as Fenton catalyst under most favorable conditions as were obtained during the optimization study. In the present study pseudo first-order kinetic model was used to analyse the kinetics of degradation [48]. The pseudo first-order rate equation is presented as below:

$$\ln(C/C_0) = -kt$$

Where, C_0 and C are the initial concentration of dye and the concentration after time t (mg L^{-1}) respectively, k is the degradation rate constant (min^{-1}). The rate constant k values can be obtained from the slope of the plots $\ln(C/C_0)$ vs t (Fig. 12). The plot $\ln(C/C_0)$ versus t showed linearity with R^2 value close to 1. Thus the degradation process accorded well with the first order kinetics. The degradation kinetics was conducted under optimized conditions from 0 to 55 min. Fig. 12 revealed that the dye degradation was initially very fast for first few minutes. In first 5 minutes of degradation operation, >79.08 % of the initial dye was degraded and then the rate of degradation slowed down. Approximately 11% of the initial dye was degraded after 50 min.

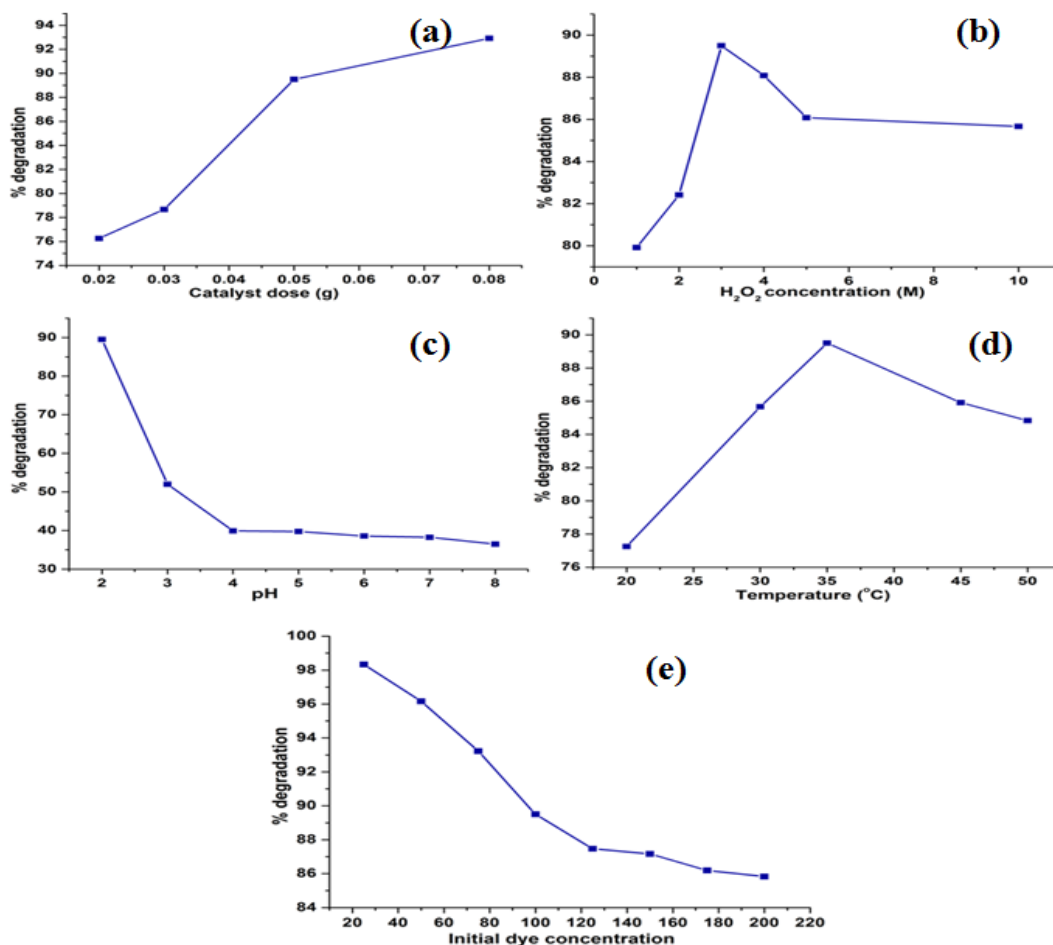


Fig. 11: (a) Effect of different parameters on dye degradation (a) catalyst dose, (b) H₂O₂ concentration, (c) pH, (d) temperature, and (e) initial dye concentration

The initial high degradation rate was due to the higher availability of free active sites at the initial stage, which declined slowly until a state of equilibrium was achieved in 55 min time. The slope of the regression line indicated that the degradation rate constant was 0.03224 min^{-1} (Fig not shown)

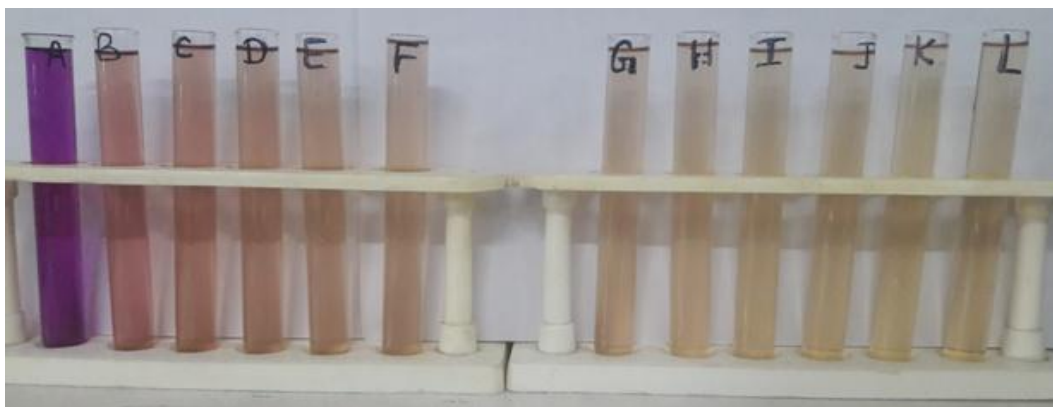


Fig. 12: Photographs of dye solutions ($100 \text{ mg} \cdot \text{L}^{-1}$) during the degradation process (A) at 0 min, (B) after 5 min, (C) after 10 min, (D) after 15 min, (E) after 20 min, (F) after 25 min, (G) after 30 min, (H) after 35 min, (I) after 40 min, (J) after 45 min, (K) after 50 min, (L) after 55 min.

Recycling of the catalyst: The catalyst was recycled under optimum degradation conditions (100 mg L^{-1} initial dye concentration, $1 \text{ ml H}_2\text{O}_2$, catalyst dose 0.05 g , and 55 min reaction time). The used catalyst was washed well with distilled water and dried for repeated use. Successive trials were repeated five times. As shown in Fig. 13, the percentage degradation of RBV dye after 55 min at each turn are 89.50% , 85.21% , 76.44% , and 49.51% respectively. The results demonstrated that the degradation capacity slightly decreased in consecutive experiments. Thus the catalyst possesses stability and recyclability up to four consecutive runs.

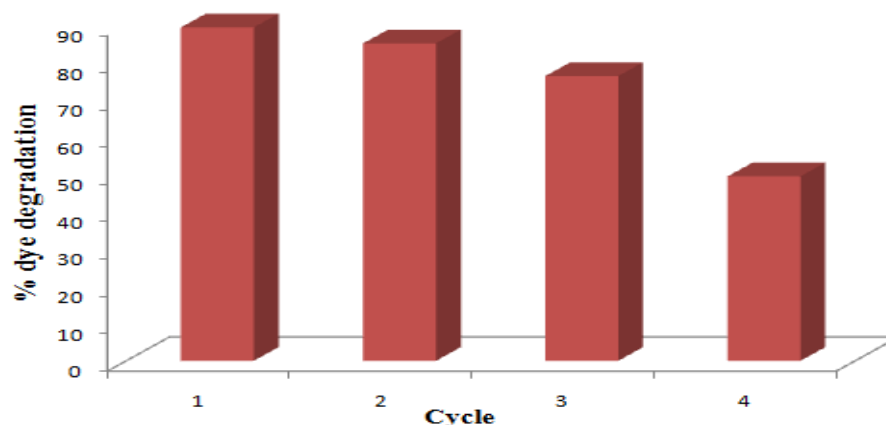


Fig. 13: Degradation efficiency (%) of catalyst after four consecutive cycles

APPLICATIONS

SFS composite behaved as an efficient heterogeneous Fentons catalyst for the degradation of Remazol Brilliant Violet dye from its aqueous solution. The catalyst is based on starch, a natural biopolymer which is, low-cost and eco-friendly.

CONCLUSIONS

The results concluded that SFS₁ in combination with H_2O_2 behaved as an effective heterogeneous catalyst for degradation of RBV dye. It is worthy to note that discoloration of RBV dye underwent fast kinetics and $\sim 90\%$ dye (from 100 mg L^{-1} dye solution) was eliminated in 55 min time using only 0.05 g of catalyst. The degradation kinetics was found to follow pseudo first order kinetic model. The catalyst can be used repeatedly for four consecutive cycles and it competently performed well over the wide range of dye concentrations. The catalyst is apparently cost effective and easily recyclable. In the future the catalyst may be evaluated for the degradation of other similar dyes.

ACKNOWLEDGEMENTS

This work was financially supported by the University Grant Commission. Authors acknowledge Indian Institute of Technology, Kanpur, India for providing the HR-TEM, EDX and FE-SEM facility. Authors thank Ewing Christian College, Allahabad for FTIR facility.

REFERENCES

- [1] R. Dandge, M. Ubale, S. Rathod, Adsorption of crystal violet dye from aqueous solution on to the surface of green peas shell (GPS), *J. Applicable.Chem.*, **2016**, 5, 792-801.
- [2] N.A. Alrazaq, A.M. Aljeboree, A.S. Alwatifi, M.B. Alqaragully, A.F. Alkaim, Removal of methylene blue dye from aqueous solutions by using date stones derived as an activated carbon, *J. Applicable.Chem.*, **2013**, 2, 788-796.

- [3] T. A. Chattree, Comparative study of adsorptive removal of red, green and violet fabric dyes from water bodies using pomegranate peel, *J. Applicable.Chem*, **2014**, 3, 2147-2156.
- [4] M. Zahmatkesh, F. Tabandeh, S. Ebrahimi, K.R.S. Sambasiva Rao, K. Farahmandi, Enhanced biodecolorization of azo dye reactive Orange 16 by immobilized phanerochaete *Chrysosporium*; Optimization of immobilization factors, *J. Applicable.Chem*, **2017**, 6, 496-506.
- [5] M. Yadav, S. Ali, O. P. Yadav, Photo-catalytic degradation of Victoria Blue-B dye using ZnS and Ag-N co-doped ZnS nanoparticles under visible radiation, *J. Applicable.Chem*, **2014**, 3, 2563-2572.
- [6] N. Gupta, H.P. Singh, R.K. Sharma, Metal nanoparticles with high catalytic activity in degradation of methyl orange: An electron relay effect, *J. Mol. Catal. A: Chem*, **2011**, 335, 248–252.
- [7] S. Bhakya, S. Muthukrishnan, M. Sukumaran, M. Muthukumar, T. Senthil Kumar, M.V. Rao, Catalytic degradation of organic dyes using synthesized silver nanoparticles: A green approach, *J Bioremed Biodeg*, **2015**, 6, 1-9.
- [8] G. Kozmaa, A. Rónavária, Z. Kónyaa, Á. Kukovecza, Environmentally benign synthesis methods of zero valent iron nanoparticles, *ACS Sustainable Chem. Eng*, **2016**,4, 291–297.
- [9] R. Yuvakkumar, V. Elango, V. Rajendran, N. Kannan, Preparation and characterization of zero valent iron nanoparticles, *Dig J Nanomater Biostruct*, **2011**, 6, 1771-1776.
- [10] H. Wu, J.J. Yin, W.G. Wamer, M. Zeng, Y. M. Lo, Reactive oxygen species-related activities of nano-iron metal and nano-iron oxides, *J Food Drug Anal*, **2014**, 22, 86 -94.
- [11] M.S. Lucas, J.A. Peres, Decolorization of the azo dye Reactive Black 5 by Fenton and photo-Fenton oxidation, *Dyes Pigm*, **2006**, 71, 236–244.
- [12] G.K. Zhang, Y.Y. Gao, Y.L. Zhang, Y.D. Guo, Fe₂O₃-Pillared rectorite as an efficient and stable Fenton-like heterogeneous catalyst for photodegradation of organic contaminants, *Environ. Sci. Technol*, **2010**, 44, 6384-6389.
- [13] Y. Zhang, K. Zhang, C. Dai, X. Zhou, H. Si, An enhanced Fenton reaction catalyzed by natural heterogeneous pyrite for nitrobenzene degradation in an aqueous solution, *Chem. Eng. J*, **2014**, 244, 438-445.
- [14] F. He, D. Zhao, Preparation and characterization of a new class of starch-stabilized bimetallic nanoparticles for degradation of chlorinated hydrocarbons in water, *Environ. Sci. Technol*, **2005**, 39, 3314-3320.
- [15] M.R. Chandraiah, Facile synthesis of zero valent iron magnetic biochar composites for Pb(II) removal from the aqueous medium, *Alexandria Eng. J*, **2016**, 55, 619–625.
- [16] N. Ezzatahmedi, G.A. Ayoko, G.J. Millar, R. Speight, C. Yan, J. Li, S. Li, J. Zhu, Y. Xi, Clay-supported nanoscale zero-valent iron composite materials for the remediation of contaminated aqueous solutions: A review, *Chem. Eng. J*, **2017**, 312, 336–350.
- [17] M. Xing, J. Wang, Nanoscaled zero valent iron/graphene composite as an efficient adsorbent for Co(II) removal from aqueous solution, *J. Colloid Interface Sci*, **2016**, 474, 119–128.
- [18] H. Dang, Y. Zhang, P. Du, Enhanced removal of soluble Cr (VI) by using zero-valent iron composite supported by surfactant-modified zeolites, *Water Sci Technol*, **2014**, 70, 1398-1404.
- [19] S.A. Kim, S. Kamala-Kannan, S.G. Oh, M. Cho, S. Bae, B.T. Oh, Simultaneous removal of chromium(VI) and Reactive Black 5 using zeolite supported nano-scale zero-valent iron composite, *Environ. Earth Sci*, **2016**, 75,447-454.
- [20] J. Zhan, T. Zheng, G. Piringner, C. Day, G.L. Mcpherson, Y. Lu, K. Papadopoulos, V.T. John, Transport characteristics of nanoscale functional zerovalent iron/silica composites for in situ remediation of trichloroethylene, *Environ. Sci. Technol*, **2008**, 42, 8871–8876.
- [21] Z. Mao, Q. Wu, M. Wang, Y. Yang, J. Long, X. Chen, Tunable synthesis of SiO₂-encapsulated zero-valent iron nanoparticles for degradation of organic dyes, *Nanoscale Res. Lett*, **2014**, 9, 501-509.
- [22] M. Baikousi, Y. Georgiou, C. Daikopoulos, A.B. Bourlinos, J. Filip, R. Zboril, Y. Deligiannakis, M.A. Karakassides, Synthesis and characterization of robust zero valent iron/mesoporous carbon composites and their applications in arsenic removal, *Carbon*, **2015**, 93, 636–647.

- [23] H. Lu, X. Qiao, W. Wang, F. Tan, Z. Xiao, J. Chen, Facile preparation of mesoporous silica/nano zero-valent iron composite for Pb(II) removal from aqueous solution, *Desalination Water Treat*, **2016**, 57, 10745–10756.
- [24] G. Liu, Y. Zhou, Z. Liu, J. Zhang, B. Tang, S. Yang, C. Sun, Efficient nitrate removal using micro-electrolysis with zero valent iron/activated carbon nanocomposite, *J. Chem. Technol. Biotechnol*, **2016**, 91, 2942–2949.
- [25] S. Bhowmick, S. Chakraborty, P. Mondal, W.V. Renterghem, S.V.D. Berghe, G.R. Ross, D. Chatterjee, M. Iglesias, Montmorillonite-supported nanoscale zero-valent iron for removal of arsenic from aqueous solution: kinetics and mechanism, *Chem. Eng. J*, **2014**, 243, 14–23.
- [26] X.Y. Jin, Z.C. Zhuang, B. Yu, Z.X. Chen, Z.L. Chen, Functional chitosan-stabilized nanoscale zero-valent iron used to remove acid fuchsine with the 981 assistance of ultrasound, *Carbohydr. Polym*, **2016**, 136, 1085–1090.
- [27] T.Y. Liu, X. Yang, Z.L. Wang, X.X. Yan, Enhanced chitosan beads-supported Fe⁰-nanoparticles for removal of heavy metals from electroplating wastewater in permeable reactive barriers, *Water Res*, **2013**, 47, 6691–6700.
- [28] M. Mosaferei, S. Nemati, A. Khataee, S. Nasser, A.A. Hashemi, Removal of Arsenic (III, V) from aqueous solution by nanoscale zero-valent iron stabilized with starch and carboxymethyl cellulose, *J Environ Health Sci Eng*, **2014**, 12, 74–84.
- [29] V. Singh, J. Singh, Preeti, A.K. Pandey, S. Joshi, L.M. Dwivedi, N. Fatima, S. Tiwari, One pot catalyzed synthesis of 1,3-bis (2-(4-hydroxyphenyl)-2-methyl-4,5-diphenyloxazol-3(2H)-yl) thiourea and its antimicrobial activity, *J. Applicable.Chem*, **2017**, 6, 688–700.
- [30] M. Pattanayak, D. Mohapatra, P.L. Nayak, Green synthesis and characterization of zero valent iron nanoparticles from the leaf extract of syzygium aromaticum (clove), *Middle East J Sci Res*, **2013**, 18, 623–626.
- [31] N. M. Aljamali, Review in azo compounds and its biological activity, *Biochem. Anal. Biochem*, **2015**, 4, 2–6.
- [32] P.D. Mines, J. Byun, Y. Hwang, H.A. Patel, H. R. Andersen, C.T. Yavuz, Nanoporous networks as effective stabilisation matrixes for nanoscale zero valent iron and groundwater pollutant removal, *J. Mater. Chem. A*, **2016**, 4, 632–639.
- [33] Z.T. Ildefonso, P.B.J.d. Jesus, T.L.C. Yunueth, L.R. Luis, M.L.M. Luisa, M.V. Yunny, A phenomenon of degradation of methyl orange observed during the reaction of NH₄TiOF₃ nanotubes with the aqueous medium to produce TiO₂ anatase nanoparticles, *RSC Adv*, **2016**, 6, 76167–76173.
- [34] J. Macias-Sanchez, L. Hinojosa-Reyes, J.L. Guzman-Mar, J.M. Peralta-Hernandez, A. Hernandez-Ramirez, Performance of the photo-Fenton process in the degradation of a model azo dye mixture, *Photochem. Photobiol. Sci*, **2011**, 10, 332–337.
- [35] J.M. Joseph, H. Destailats, H.M. Hung, M.R. Hoffmann, The sonochemical degradation of azobenzene and related azo dyes: Rate enhancements via Fenton's reactions, *J. Phys. Chem. A*, **2000**, 104, 301–307.
- [36] S. Garg, A.K. Jana, Effect of propylation on the characteristics of corn starch and variation of properties with different degrees of substitution, *J. Appl. Polym. Sci*, **2011**, 119, 1383–1392.
- [37] V. Singh, P. Kumar, Design of nanostructured tamarind seed kernel polysaccharide-silica hybrids for mercury (II) removal, *Sep. Sci. Technol*, **2011**, 46, 825–838.
- [38] Z. Olejniczak, M. Leczka, K.C. Kowalska, K. Wojtach, M. Rotika, W. Mozgawa, ²⁹Si MAS, NMR and FTIR study of inorganic-organic hybrids gels, *J. Mol. Struct*, **2005**, 744–747, 465–471.
- [39] Z. Guo, L.L. Henry, V. Palshin, Elizabeth J. Podlaha, Synthesis of poly(methyl methacrylate) stabilized colloidal zero-valence metallic nanoparticles, *J. Mater. Chem*, **2006**, 16, 1772–1777.
- [40] O. Odeku, K. Picker, Analysis of the material and tablet formation properties of four Dioscorea Starches, *Starch/Stärke*, **2007**, 59, 430–444.
- [41] Y.M. Xu, W.P. Du, Y.S. Wang, Photoinduced degradation of orange II on different iron (Hydr) oxides in aqueous suspension: rate enhancement on addition of hydrogen peroxide, silver nitrate, and sodium fluoride, *Langmuir*, **2008**, 24, 175–181.

- [42] H.P. He, X.L. Liang, Y.H. Zhong, S.Y. Zhu, J.X. Zhu, P. Yuan, J. Zhang, The decolorization of Acid Orange II in non-homogeneous Fenton reaction catalyzed by natural vanadium-titanium magnetite, *J. Hazard. Mater.*, **2010**, 181, 112–120.
- [43] K. Dutta, S. Mukhopadhyay, S. Bhattacharjee, B. Chaudhuri, Chemical oxidation of methylene blue using a Fenton-like reaction, *J. Hazard. Mater.*, **2001**, 84, 57–71.
- [44] H. Zhang, H.J. Choi, C.P. Huang, Optimization of Fenton process for the treatment of landfill leachate, *J. Hazard. Mater.*, **2005**, 125, 166–174.
- [45] A.A. Burbano, D.D. Dionysiou, M.T. Suidan, T.L. Richardson, Oxidation kinetics and effect of pH on the degradation of MTBE with Fenton reagent, *Water Res.*, **2005**, 39, 107–118.
- [46] Q.Q. Chen, P.X. Wu, Z. Dang, N.W. Zhu, P. Li, J.H. Wu, X.D. Wang, Iron pillared vermiculite as a heterogeneous photo-Fenton catalyst for photocatalytic degradation of azo dye reactive brilliant orange X-GN, *Sep. Purif. Technol.*, **2010**, 71, 315–323.
- [47] J.H. Ramirez, C.A. Costa, L.M. Madeira, Experimental design to optimize the degradation of the synthetic dye Orange II using Fenton's reagent, *Catal. Today*, **2005**, 107–108, 68–76.
- [48] B. Cuiping, G. Wenqi, F. Dexin, X. Mo, Z. Qi, C. Shaohua, G. Zhongxue, Z. Yanshui, Natural graphite tailings as heterogeneous Fenton catalyst for the decolorization of rhodamine B, *Chem. Eng. J.*, **2012**, 197, 306–313.

AUTHORS' ADDRESSES

1. **Jadveer Singh**

Department of Chemistry,
University of Allahabad, Allahabad-211002
Mobile: 9804950395, E-mail: jadveer007@gmail.com

2. **Dr. Preeti**

Department of Chemistry,
University of Allahabad, Allahabad-211002
Mobile: 8081280654, E-mail: preetisrivastava.au@gmail.com

3. **Prof. Vandana Singh**

Department of Chemistry,
University of Allahabad, Allahabad-211002
Mobile: 7007182033, E-mail: vschemau@gmail.com